IEEE Access
Multidisciplinary ⋮ Rapid Review ⋮ Open Access Journal

Received July 3, 2021, accepted July 19, 2021, date of publication July 26, 2021, date of current version July 30, 2021.

Digital Object Identifier 10.1109/ACCESS.2021.3099255

Development and Assessment of Improved Global Pressure and Temperature Series Models

JIAN MAO[1,2], JUNYANG HAN[1], AND TIEJUN CUI[1,2]

[1]School of Geographic and Environmental Sciences, Tianjin Normal University, Xiqing, Tianjin 300387, China
[2]Tianjin Engineering Center for Geospatial Information Technology, Tianjin Normal University, Tianjin 300387, China

Corresponding author: Tiejun Cui (tiejuncui@163.com)

ABSTRACT Global pressure and temperature (GPT) series models can provide the underlying meteorological parameters for tropospheric corrections without any other meteorological observations, which allows them to be widely used for a series of geodetic as well as meteorological and climatological purposes. Due to the height difference between the empirical model height and user location, a vertical correction of meteorological parameters is inevitable, particularly for airborne users. Unfortunately, the GPT series models have limitations on the vertical correction. We explored the temperature lapse rate for the vertical adjustment using 10 years of reanalysis data provided by the National Centers for Environmental Prediction (NCEP), and extended the GPT models to improved global pressure and temperature (IGPT) series models by introducing a new temperature lapse rate model and a new formulation of pressure reduction. An evaluation of the IGPT models expression determines that the IGPT models have better accuracy than the GPT models, particularly under large height differences, which is attributed to their ability to consider the real behavior of temperature in the atmosphere and adiabatic effects on air pressure. The performance of the IGPT models in zenith tropospheric delay (ZTD) estimations was also evaluated by comparison with the fifth-generation European Centers for Medium-Range Weather Forecasts (ECMWF) Re-Analysis (ERA5) data and International GNSS Service (IGS) data. The results confirm that our new models can effectively improve the accuracy of ZTDs, particularly at larger altitude differences between the target height and the corresponding four grid points of the model, not only enhancing the performance of the model in complex terrain but also extending the feasibility of the IGPT models from the Earth's surface to higher altitudes.

INDEX TERMS GPT series models, zenith tropospheric delay, temperature lapse rate, pressure reduction.

I. INTRODUCTION

The incorrect modeling of troposphere delays is one of the major error sources for space geodetic techniques such as global navigation satellite systems (GNSS) or very long baseline interferometry (VLBI) [1]. In recent years, many accurate tropospheric delay models have been proposed based on numerical weather prediction (NWP) data, e.g., TropGrid series models [2], [3], global pressure and temperature (GPT) series models [1], [4]–[6], and IGGtrop series models [7], [8]. The GPT series models characterized by high accuracy are the most widely used in meteorological and geodetic applications.

The associate editor coordinating the review of this manuscript and approving it for publication was Stefania Bonafoni.

The GPT model was developed by Boehm [4], and can provide pressure and temperature at any site in the vicinity of the Earth's surface in the form of spherical harmonics. The meteorological parameters are derived as the mean values and annual amplitudes from 3 years of global monthly mean profiles for pressure and temperature provided by the European Centre for Medium-Range Weather Forecasts (ECMWF). However, it can only estimate zenith hydrostatic delays (ZHD) using the equation given by Saastamoinen [9]:

$$ZHD = \frac{0.0022768P}{1 - 0.00266\cos(2\phi) - 0.00000028H} \quad (1)$$

where P is the air pressure at the station, ϕ is the station geodetic latitude and H is the station height.

To improve the limited spatial and temporal variability of the GPT model, Lagler *et al.* [4] proposed a more advanced

TABLE 1. Overview of GPT series models.

Model	Temporal resolution	Spatial resolution	Parameter	Hydrostatic delay model	Wet delay model
GPT2	day	5°	p, T, Q, dT, a_h, a_w	Saastamoinen	Saastamoinen
GPT2w	day	1°,5°	$p, T, Q, dT, T_m, \lambda, a_h, a_w$	Saastamoinen	Askne & Nordius
GPT3	day	1°,5°	$p, T, Q, dT, T_m, \lambda, a_h, a_w, G_{nh}, G_{eh}, G_{nw}, G_{ew}$	Saastamoinen	Askne & Nordius

troposphere model, namely, GPT2. The six model output parameters (air pressure P, temperature T, temperature lapse rate dT, specific humidity Q, and dry and wet mapping function coefficients a_h and a_w, respectively) are derived by statistical analysis of monthly mean ERA-Interim profiles over the time period 2001 to 2010. These internally derived parameters r are provided as average values (A_0) as well as amplitudes of annual (A_1, B_1) and semiannual (A_2, B_2) variations on a global 5° grid as follows:

$$r(t) = A_0 + A_1 cos\left(\frac{doy}{365.25}2\pi\right) + B_1 sin\left(\frac{doy}{365.25}2\pi\right) + A_2 cos\left(\frac{doy}{365.25}4\pi\right) + B_2 sin\left(\frac{doy}{365.25}4\pi\right) \quad (2)$$

where doy is the day of year. In contrast to the GPT models, the temperature lapse rate is no longer a constant but rather a period function, and the wet delay model provided by Saastamoinen is added to the GPT2 model. The GPT2 model height scaling of the surface values T, P, and the water vapor pressure e is realized by means of the temperature lapse rate dT, mean gravity g_m and virtual temperature T_v derived from the given input parameters T and Q as follows:

$$T_r = T + dT \cdot \Delta h \quad (3)$$

$$P_r = P \cdot exp(-\frac{g_m \cdot dMtr}{R_g \cdot T_v} \cdot \Delta h) \quad (4)$$

$$T_v = T(1 + 0.6077 \cdot Q) \quad (5)$$

$$e_r = \frac{Q \cdot P_r}{(0.622 + 0.378 \cdot Q)} \quad (6)$$

where T_r, P_r and e_r are the temperature, pressure and water vapor pressure at the receiver height, respectively, Δh is the height difference between the surface and receiver height, $dMtr$ is the molar mass of dry air, and R_g is the universal gas constant.

The GPT2w troposphere model is an enhancement of the GPT2 model. The extension, 'w', is related to the new wet delay model developed by Askne and Nordius [10]:

$$ZWD = 10^{-6}(k_2' + k_3/T_m)\frac{R_d}{(\lambda + 1)g_m}e \quad (7)$$

where k_2' and k_3 represent empirically determined refractivity constants, R_d is the specific gas constant of dry air, λ is the vapor pressure decrease factor, and T_m is the weighted mean temperature. These two additional parameters are provided as average values as well as amplitudes of annual and semiannual variations on a global 1° grid. In contrast to the GPT2 model, the vertical extrapolation (6) for e is replaced by the expression [10]:

$$e_r = e(\frac{P_r}{P})^{\lambda+1} \quad (8)$$

More recently, the GPT3 model, the successor of the GPT2w model, was developed by Landskron and Böhm [6]. Both models are based on the same data, where the meteorological quantities from the GPT2w model are left unchanged for the GPT3 model. The main changes are the introduction of new components, namely the hydrostatic and wet empirical mapping function coefficients derived from the special averaging techniques of Vienna Mapping Function 3 (VMF3) data. Additionally, horizontal gradient parameters (i.e., hydrostatic north gradient G_{nh}, hydrostatic east gradient G_{eh}, wet north gradient G_{nw} and wet east gradient G_{ew}) are introduced to model azimuthal asymmetry. The main characteristics of the described GPT series models are summarized in **Table 1.** It needs to be emphasized that, with the development of GPT series models, the values of meteorological parameters (i.e., p, T, Q *and* dT) in each model have been updated by the newest model, which is verified by our previous experiments.

With the widespread use of GPT series models, many relevant studies have emerged to improve or validate the performance of these models [11]–[22]. However, most validations are conducted at the surface rather than at higher altitudes. Since troposphere empirical models should be applicable for aviation, performance at higher altitudes must also be guaranteed. Unfortunately, the results of some previous studies show that the GPT series models have a poor performance in vertical corrections with increasing altitude [23]–[25]. Therefore, in the following section, we explore the causes of the shortcomings in the vertical correction, and introduce an easy way to improve the performance in the vertical extrapolation of GPT series models. The next section describes the development of this approach, which is then validated against meteorological parameters from radiosonde data and zenith delays from NWP data and GNSS observations.

II. ANALYSIS OF THE VERTICAL CORRECTION FOR GPT SERIES MODELS AND THEIR IMPROVEMENTS

As temperature and pressure are fundamental variables in GPT series models, understanding temperature lapse rates and pressure profiles is important for the extrapolation of temperature and pressure to the target height. Therefore,

we assessed the performance of the temperature lapse rate model and pressure reduction method in GPT series models, and then proposed an optimized solution for all of them. As mentioned above, all GPT series models have the same values of p, T, Q and dT but with two different spatial resolutions (i.e., 1° and 5°; see **Table 1**). Thus, we use GPT_1 and GPT_5 to represent the GPT2, GPT2w, or GPT3 models with 1-degree and 5-degree grids, respectively.

A. ANALYSIS OF THE TEMPERATURE LAPSE RATE MODEL IN GPT SERIES MODELS

To evaluate the temperature lapse rate in GPT_1 and GPT_5, we analyzed their values on a global scale first. The mean dT in GPT_1 and GPT_5 at all grid points are depicted in Fig. 1. The mean value distribution of both models shows typical land-sea differences; e.g., many positive values appear in the polar regions and west coasts of Africa and America, particularly in Antarctica, where the maximum value occurs (with a value up to 18.6 $K \cdot km^{-1}$), whereas negative values of approximately -9 $K \cdot km^{-1}$ appear in sea areas (see Fig. 1(a, b)). Additionally, the mean value histogram of both models shows a right skewed shape; a value of approximately -9 $K \cdot km^{-1}$ overwhelms the other values (see Fig. 2(a, b)), and the percentage reaches 20.9%. From the above analysis, it can be concluded that the mean dT fields of both models clearly show odd values with respect to the average value of $-6.5K \cdot km^{-1}$ in the troposphere. This is mainly caused by the fact that the dT in GPT series models is derived from the lowest two pressure levels of the ECMWF data, which limits their applications to the lower atmosphere.

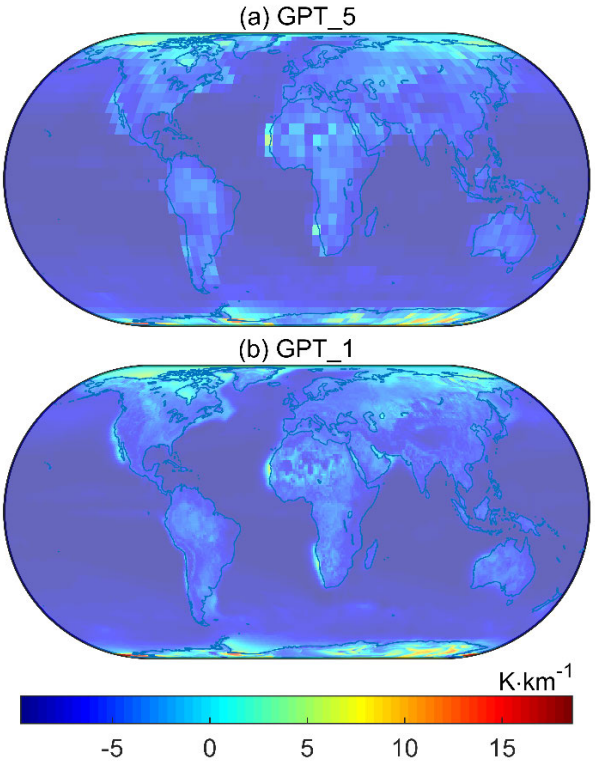

FIGURE 1. Global distribution of the annual average *dT* for GPT_1 and GPT_5: (a) global distribution of the annual average of *dT* for GPT_5; and (b) global distribution of the annual average of *dT* for GPT_1. (unit: $K \cdot km^{-1}$).

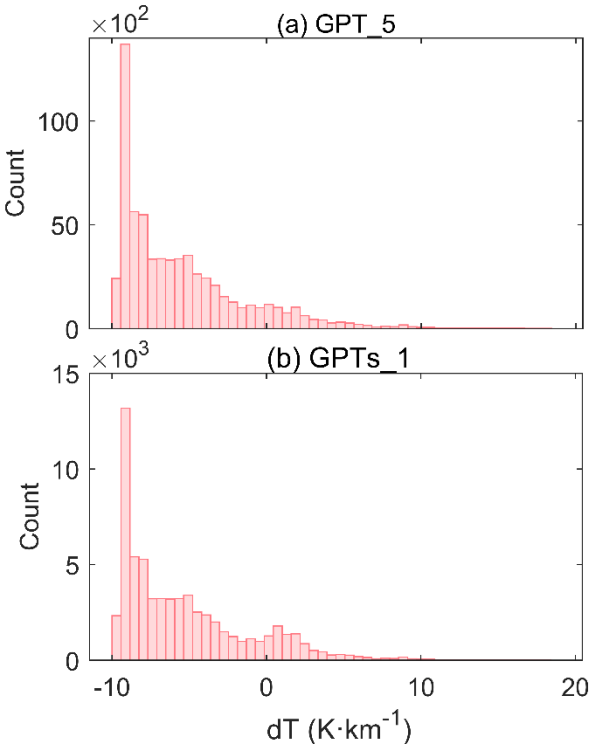

FIGURE 2. Histograms of the annual average of *dT* for GPT_1 and GPT_5: (a) histogram of the annual average *dT* for GPT_5; and (b) histogram of the annual average *dT* for GPT_1. (unit: $K \cdot km^{-1}$).

B. DETERMINATION OF THE NEW TEMPERATURE LAPSE RATE MODEL

Therefore, an accurate dT model is needed to overcome the abovementioned limitation. For this study, 10 years (January 1, 2008 to December 31, 2017) of the final analyses (FNL) of the Global Data Assimilation System (GDAS) model was chosen for dT modeling, as provided by the National Centre for Environmental Prediction (NCEP). The NCEP reanalysis data are three-dimensional meteorological fields with a horizontal resolution of 1°× 1° as well as 6 h temporal resolution and 31 vertical layers (up to approximately 48 km). The dT values of each grid point at a certain moment should be calculated. dT can be estimated as a coefficient for a function of temperature and height by least-squares fitting. The fitted function is as follows:

$$T = dT \cdot H + b \tag{9}$$

where T is the temperature, H is the corresponding height of T, and b is the intercept. It needs to be emphasized that the height H in lapse rate fitting is up to the tropopause (approximately 11 km).

After obtaining the long-term (10 years) values of dT for each grid point of the NCEP data, the variation characteristics

of these time series data were analyzed with the fast Fourier transform for each grid point. Fig. 3 illustrates the stacked power spectral density of dT. Clearly, the 6-h sampled time series contains significant annual, semiannual and diurnal peaks for the lapse rate. Consequently, considering that the new dT model should be easy to use and therefore applicable to all GPT models, we used a periodic function only with an annual period to establish empirical models for dT. The periodic function proposed by Niell [26] is expressed as:

$$a = a_0 + A \cdot cos(\frac{doy - 28}{365.25}2\pi) \tag{10}$$

where a_0 is the mean value, A is the annual amplitude, and doy is the day of the year.

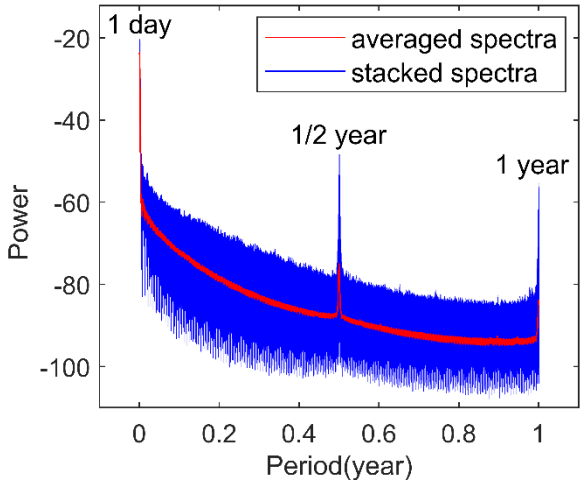

FIGURE 3. Stacked spectra of dT for a set of 360 × 181 grid points over 10 years with the mean value of powers. It shows significant annual, semiannual and diurnal variations for dT.

Based on (10), the coefficients of a_0 and A of dT were estimated by using least-squares fitting. Fig. 4 illustrates the mean values of dT and the latitudinal variations in their longitudinally averaged values. The distributions of these mean values show remarkable north-south symmetrical distributions with the peak in the tropics while decreasing toward the poles. However, they are also characterized by evident regional variation; e.g., large values mainly appear in drylands, such as the Arabian Peninsula, North Africa, the western side of the North American continent, and northern Chile. The ranges of dT are from -2.7 to -7.0 K·m^{-1}, which seems to be closer to reality with respect to those of dT in GPT series models.

Subsequently, aiming at proposing an easy-to-implement and operable vertical correction method for all GPT series models, a piecewise linear function was used to model dT. The breakpoints of this piecewise linear function are determined according to the actual state of the atmosphere. Fig. 5 depicts the dividing results of dT along latitude, showing piecewise linear function curves with breakpoints generated according to the inflection points of the

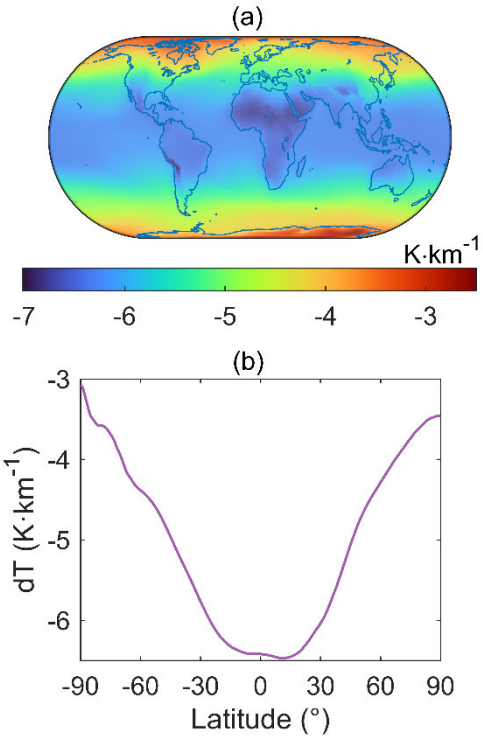

FIGURE 4. Global distribution of the annual average of dT in $K \cdot km^{-1}$ (a) and latitudinal variations in the longitudinally averaged values of dT (b). It shows that the distribution of dT is notably latitude dependent.

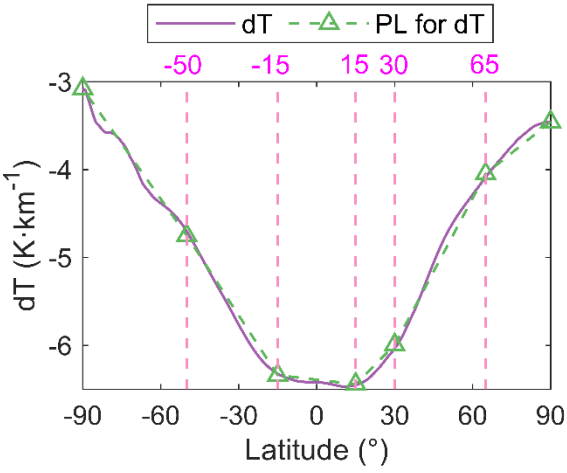

FIGURE 5. Piecewise linear function curves of dT (purple solid line) with breakpoints generated according to the inflection points of the dT-latitude (green dotted line).

dT-latitude curve. We can see that the piecewise linear function is divided into 6 segments on the intervals, namely, [−90 −50], [−50 −15], [−15 15], [15 30], [30 65] and [65 90], which provides a good account of the actual latitudinal variation in dT. According to the dividing results, we adopted a look-up table of the meteorological parameters to account for the seasonal and latitudinal variations in neutral atmospheric behavior. **Table 2** shows the look-up table of dT,

TABLE 2. Average and amplitude values for the new temperature lapse rate model.

	Temperature Lapse Rate($K \cdot km^{-1}$)	
Latitude	Average(a_0)	Amplitude(A)
90	-3.46	-0.07
65	-4.05	0.46
30	-5.99	0.38
15	-6.44	0.07
-15	-6.34	-0.10
-50	-4.75	0.05
-90	-3.08	0.79

where the data are divided into two groups to account for the annual mean and amplitude of each parameter. The interpolation between latitudes for dT is performed with a linear function as follows:

$$Vc_{\emptyset} = Vc_i + \frac{Vc_{i+1} - Vc_1}{L_i}(\phi - Lat_i), \times \phi_i \in [La_i, Lat_{i+1}], Mc \in \{a_0, A\} \quad (11)$$

where $Vc_{\emptyset}$ and Vc_i denote seasonal variation coefficients from the mean data set of a_0 or the amplitude data set of A, ϕ is the latitude of the site, i denotes the i-th interval, L_i is the length of the i-th interval, and Lat_i is the latitude of the i-th interval. After calculating the annual mean and amplitude values, the value of dT for latitude ϕ and day of year doy can be obtained as:

$$dT(\phi, doy) = Vc_{\phi}^{a_0} + Vc_{\phi}^{A}\left(\cos\left(\frac{doy - 28}{365.25}2\pi\right)\right) \quad (12)$$

C. VALIDATION OF THE NEW TEMPERATURE LAPSE RATE MODEL

To assess the newly proposed dT model along with those in GPT series models and the UNB3 model, we compared the lapse rates calculated by the models with those derived from RS data. Considering the distribution of the atmospheric temperature, the difference between the planetary boundary layer (from the Earth's surface to a height of 1∼2 km) and free atmosphere (above the planetary boundary layer), temperature lapse rates measured close to surfaces can differ substantially from the free-air lapse rate [27]. Moreover, the dT of GPT series models is derived from the lowest two pressure levels of the ECMWF data. Therefore, we chose ten schemes with different height levels (from 1 to 10 km upon the surface) to fit the lapse rate. A total of 512 globally distributed RS stations data in 2019 were selected to estimate lapse rates for the ten schemes, which were used as references.

The two statistical quantities, namely, the Bias and root mean square error (RMSE), were selected to measure their performance, which can be calculated via the following equations:

$$Bias = \frac{1}{N}\sum_{i=1}^{N}(V_{model}^{i} - V_{reference}^{i}) \quad (13)$$

$$RMSE = \sqrt{\frac{1}{N}\sum_{i=1}^{N}(V_{model}^{i} - V_{reference}^{i})^2} \quad (14)$$

where V_{model}^{i} and $V_{reference}^{i}$ are the values from the models and reference data, respectively, and N is the number of samples. The statistical results are shown in Fig. 5.

As can be observed in Fig. 6(a), the new dT model tends to have negative Biases at almost all levels, whereas the Biases of other models show similar trends, having negative Bias below the fitting height level of 5 km but positive Bias above that level. The largest Bias of each model appears at the 1 km fitting height and the value reaches up to $-1.37\ K \cdot km^{-1}$ for the UNB3 model. In terms of RMSE (see Fig. 6(b)), the values of both the new and UNB3 models decrease with increasing fitting height, but the RMSEs of the new model are smaller than those of UNB3 at all fitting levels. However, the RMSE values of the GPT series models are stable at

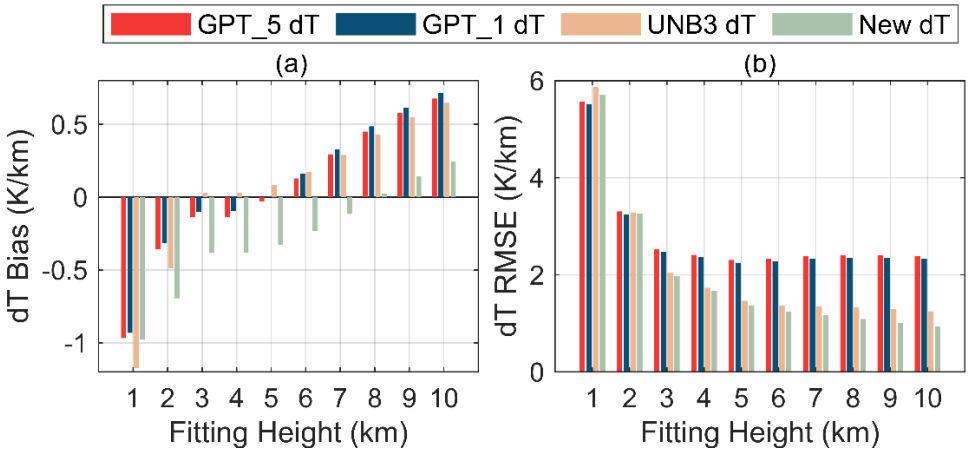

FIGURE 6. Average Biases and RMSEs of different dT models at different fitting height levels assessed with dT derived from radiosonde data. (a): Biases at different levels (unit: $K \cdot km^{-1}$); and (b): RMSEs at different levels (unit: $K \cdot km^{-1}$).

approximately 2.3 $K \cdot km^{-1}$ at fitting height levels above 3 km, where the values of the GPT series models are obviously larger than those of the new and UNB3 models. For GPT series models, the accuracy of dT in the lower atmosphere does not benefit from using the lowest two pressure levels to obtain lapse rates. Its lowest accuracy of 5.5 $K \cdot km^{-1}$ appears at a height level of 1 km, probably because the primary determinant of surface temperatures is the local surface energy balance (net radiative and turbulent heat flux) [27]–[29], which results in drastic changes in lapse rates in time and space, whereas both GPT_5 and GPT_1 cannot accurately describe the spatial-temporal patterns of lapse rate variability near the surface. Statistics were conducted to calculate the average RMSE of all schemes. The results show that the average RMSEs are 2.8 $K \cdot km^{-1}$, 2.7 $K \cdot km^{-1}$ and 2.1 $K \cdot km^{-1}$ for GPT_5, GPT_1 and UNB3, respectively. The new dT model has an average RMSE of 1.9 $K \cdot km^{-1}$; thus, the new model achieves precision improvements of approximately 32%, 30% and 10% compared with GPT_5, GPT_1 and UNB3, respectively.

D. IMPROVEMENT OF THE PRESSURE REDUCTION FOR GPT SERIES MODELS

The pressure reduction of all GPT series models uses exponential trend coefficients calculated from grid pointwise virtual temperature information; see (4). These isothermal scale heights may be alternatively adjusted for adiabatic effects at low altitude, but the benefit of this approach is not entirely conclusive [1]. For convenience, this method is named the isothermal model in this paper. In fact, the atmosphere is not isothermal, where the air temperature falls very noticeably with increasing altitude. Therefore, using the isothermal model will inevitably produce a large bias with respect to the pressure reduction at high altitudes and therefore result in a poor performance in ZTD corrections.

To overcome this problem, we use the formula given by Kleijer [30] instead of (4):

$$P_H = P(1 + \frac{dT \cdot \Delta h}{T})^{\frac{-g_m}{R_d dT}} \tag{15}$$

where dT is the temperature lapse rate, T is the temperature at the grid points, R_d is the specific gas constant of dry air, and the other parameters are consistent with (4). This expression was proposed based on the assumption of an adiabatic atmosphere where temperature changes with altitude due to adiabatic processes driven by the vertical movement of air parcels, which makes it more realistic than (4) in modeling the atmospheric structure of the troposphere. Thus, we named this method the adiabatic model in this paper.

To justify the adiabatic model, three stations were isolated to visualize their pressure profiles. The selection was made to have a sample with different latitudes. Stations 89002 (Neumayer), SBPV (Porto Velho, Brazil), and PABR (Barrow, USA) at latitudes 70.7° S, 8.8° S, and 71.3° N, respectively, were chosen. Using the vertical as well as positional and temporal information of these three stations, we deployed the isothermal model, adiabatic-GPT model (with dT from GPT_1) and adiabatic-new model (with dT from the new lapse rate model), to obtain predictions of the pressure. The surface pressure, temperature and specific humidity derived from RS data were used to obtain pressure profiles for the two models. The pressure residual profiles derived from the models minus RS in different seasons are plotted in Fig. 7. With increasing altitude, the residual values of the isothermal model and adiabatic-GPT model vary greatly and present a systematic error, whereas those of the adiabatic-new model are relatively stable and small. Benefitting from the new dT and adiabatic model, the adiabatic-new model obviously outperforms the isothermal and adiabatic-GPT models. This finding confirms again that the new dT model has better accuracy than GPT series models, describing the vertical distribution of temperature more reliably.

Having shown the good performance of the new dT model, we use it to replace the original dT model in GPT series models. Moreover, the adiabatic model is also introduced into GPT series models. Here, the improved GPT series models are denoted as IGPT.

III. VALIDATION OF THE IGPT SERIES MODELS

In this section, we compare the IGPT models with the GPT models in terms of meteorological parameters against the radiosonde data of 512 stations distributed all over the Earth. Then, the accuracy of the ZTDs estimated by the two types of models is assessed by using the ZTDs derived from ERA5 data with a spatial resolution of $1° \times 1°$. Furthermore, the superiority of the new model for usage in geodetic applications is demonstrated by global GNSS solutions.

A. COMPARISON OF METEOROLOGICAL PARAMETERS TO RADIOSONDE DATA

The data from 512 globally distributed radiosonde stations in 2019 were selected again as a reference to validate the IGPT models. Values of meteorological parameters (air pressure, temperature and specific humidity, which is converted to water vapor partial pressure) are given as vertical profiles with 30–70 different height levels. Considering the improvement effects on the vertical extrapolation of T, P, and e, we chose these three meteorological parameters to validate the IGPT models. The meteorological parameters provided by the RS data and models (i.e., GPT and IGPT) were compared not only at the surface level but also vertically at different heights. The vertical profile was divided into 11 levels (from the surface to 10 km by 1 km) to unify the representation of the data. Since the values of the RS data are at different levels, we interpolate temperature and specific humidity at each height level with a linear function and extrapolate pressure with (15) from the nearest height level.

Fig. 8 provides the statistical results at all levels for the GPT and IGPT models. As seen in Fig. 8(a), the pressure Bias values of both GPT_5 and GPT_1 are positive and increase along the entire height range with increasing height.

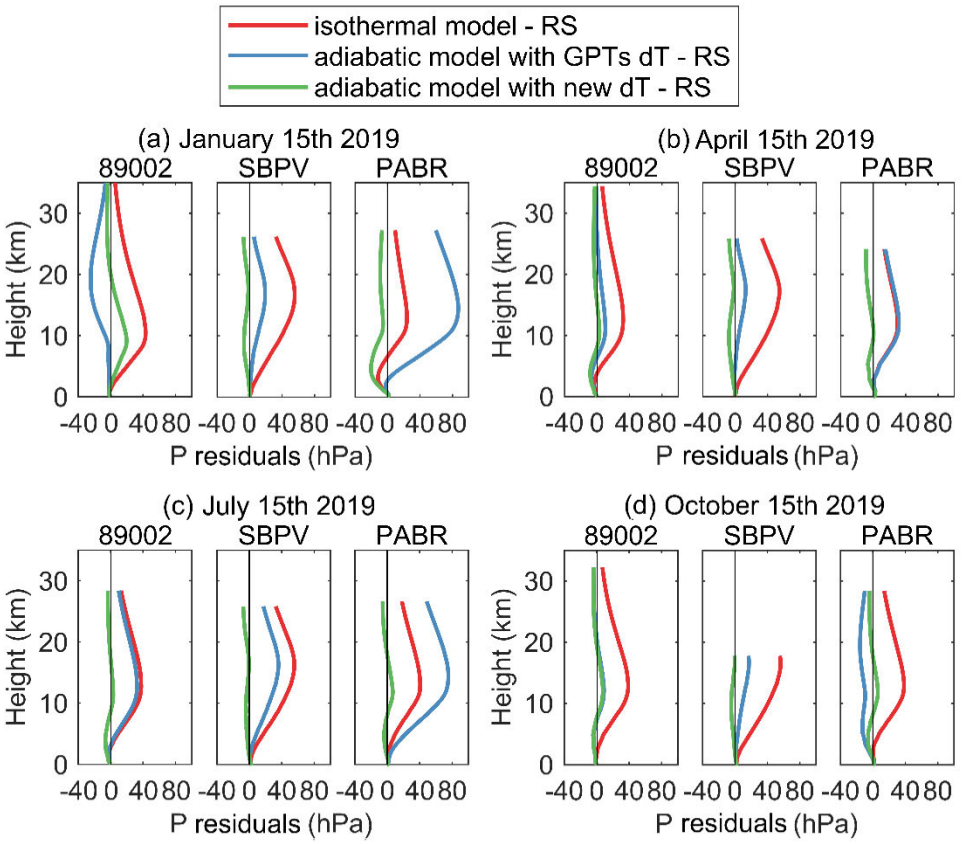

FIGURE 7. Pressure residual profiles of station 89002, SBPV and PABR in different seasons as provided by RS and as determined with the empirical models from the isothermal, adiabatic-GPT (with *dT* from GPT_1) and adiabatic-new (with *dT* from the new lapse rate model) models. (Unit: hPa). (a): P residuals on January 15th 2019; (b): P residuals on April 15th 2019; (c): P residuals on July 15th 2019; and (d): P residuals on October 15th 2019.

This implies that the GPT models with the isothermal model overestimate the pressure, particularly at higher altitudes. The RMSE values of both GPT_5 and GPT_1 for all meteorological parameters are very close to those of the IGPT models at the surface level, but with increasing altitude, they increase significantly in P and T (see Fig. 8(b, d)). In contrast, the Bias and RMSE values of the IGPT models are relatively stable and small. The IGPT models clearly mitigate the discrepancies existing between the GPT models and meteorological observations at higher altitudes over the entire globe. In particular, the IGPT models provide an excellent dT model and the adiabatic model for pressure reductions that account for the substantial reduction of the Bias and RMSE values at an altitude of 10 km; e.g., the mean RMSEs of P of IGPT_5 and IGPT_1 are reduced by 30.0 hPa (from 38.0 to 8.0 hPa) and 30.2 hPa (from 38.3 to 8.1 hPa), respectively, and those of T are reduced by 11.8 K (from 20.8 to 9.0 K) and 11.4 K (from 20.4 to 9.0 K), respectively.

In terms of water vapor pressure, large negative values of Bias for all models were observed at lower altitudes, which indicates an underestimation of the GPT-derived surface e (see Fig. 8(e)). Moreover, the Bias values of all models tend to increase positively with height, but the increase in the Bias of the GPT models is greater than that of the IGPT models. This is rooted in the isothermal model used in the GPT model which leads to the overestimation of P, and consequently to overestimating e according to (8). Although the IGPT models have overcome this problem by using the adiabatic model, due to the systematic underestimation of e at the surface, the RMSE values of e are close to or greater than those of the GPT models within a height range of 0∼4 km (see Fig. 8(f)). However, as the e underestimated influence weakens with increasing altitude, the RMSE values of e are smaller than those of the GPT models at a high altitude (e.g., 5∼10 km); see Fig. 8(f).

The statistical results of the Bias and RMSE between the model-derived and RS-derived pressures at the 10 km level are shown in Fig. 9, in which the spatial variation in the accuracy of the two types of models can be seen. From this, it can be concluded that the GPT models obviously overestimate the pressure at all stations with an average Bias of 37.4 hPa and 37.7 hPa for GPT_5 and GPT_1, respectively, whereas the IGPT models (i.e., IGPT_5 and IGPT_1) have the same average Bias of 1.4 hPa, achieving a 96% improvement. Nevertheless, the Bias distribution of the IGPT models is approximately latitude dependent; e.g., negative

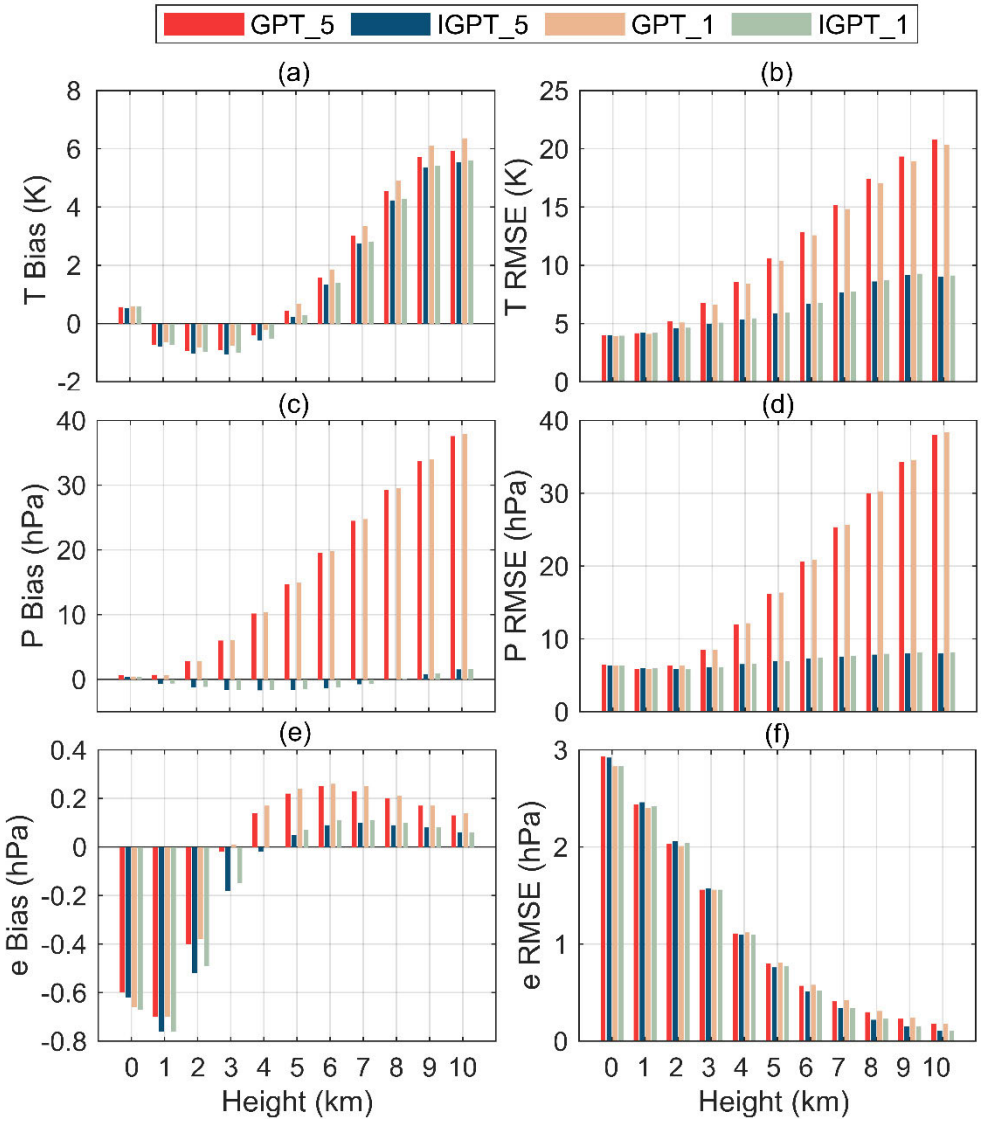

FIGURE 8. Results of the GPT and IGPT models for the meteorological parameter estimations per level. It shows that the accuracy of *P* and *T* for the GPT models varies significantly with increasing altitude, whereas those of the IGPT models are stable and small with increasing altitude. (a): Biases of *P* at different levels (unit: hPa); (b): RMSEs of *P* at different levels (unit: hPa); (c) Biases of *T* at different levels (unit: K); (d): RMSEs of *T* at different levels (unit: K); (e) Biases of *e* at different levels (unit: hPa); and (f): RMSEs of *e* at different levels (unit: hPa).

Biases appear in the tropics, whereas positive Biases appear in the polar regions. For GPT series models, the RMSE shows similar characteristics to the Bias on a global scale, and their values are fairly close to each other. This implies that a significant part of the error in the pressure reduction is due solely to the persistent bias. After the improvement, the RMSE of each RS station has clearly reduced giving a mean of 8.2 hPa, a very respectable result.

Analogously, Fig. 10 displays the distributions of the Bias and RMSE for the temperature at the 10 km level. Unlike the pressure, the Bias of the GPT models is evidently characterized by land-sea differences with positive values over continental areas and negative values along seacoasts. The differences in T vary between -37.5 K and 78.9 K with a maximum in the Arctic, probably linked to its dT model designed only for the correction of near-surface measurements, which also leads to enlarged total mean RMSEs of 20.8 K and 20.4 K for GPT_5 and GPT_1, respectively. An accuracy of better than 10 K was achieved at most stations for the IGPT models, and the percentage reached 55% and 53% for IGPT_5 and IGPT_1, respectively. Moreover, the mean RMSEs of IGPT_5 and IGPT_1 are equivalent, with a value of 9 K, achieving a 57% improvement.

Since almost no water vapor remains at the 10 km level, the Biases and RMSEs of e for all models are small and vary slightly among the globally distributed RS stations; see Fig. 11. However, the statistical results of e from the IGPT models, including RMSEs and Biases, are better than those

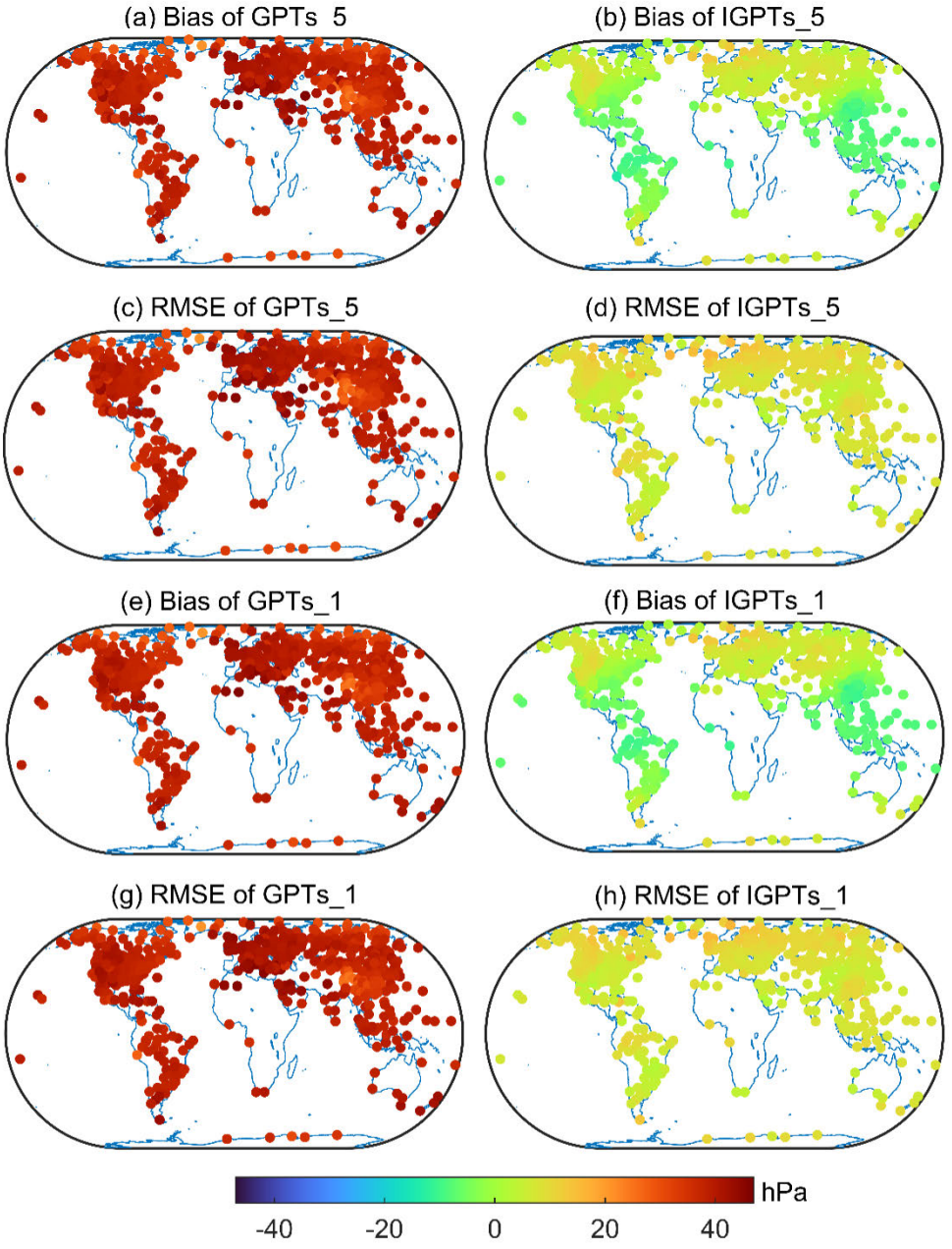

FIGURE 9. Biases and RMSEs of the differences between the RS-derived and model-derived *P* from GPT minus RS and IGPT minus RS, calculated for 512 RS stations at the 10 km level in 2019 (unit: hPa).

of the GPT models, particularly over the tropical region (e.g., South Asia and northern South America). This demonstrates that the IGPT models profit from the new dT model and the optimized pressure reduction which allow for describing the vertical distribution of the water vapor more reliably.

B. COMPARISON OF ZTDs TO ERA5 DATA

To compare the ZTDs with the ERA5 data, we need to calculate ZTD_{ERA5} from the vertical profiles first. The ERA5 data are in the form of three-dimensional matrices with 37 vertical pressure levels, which make it possible to obtain the ZTD as an integral from the refractivity. Therefore, the integration method proposed by Wilgan *et al.* [31] was applied through the pressure-level data to obtain the tropospheric delays. A thorough description of this approach is given in that reference.

The integration method applied in the ZTD_{ERA5} calculation allows us to separate the wet delay from the hydrostatic delay. Therefore, it is possible to validate the performance of the IGPT models in predicting the ZHDs and ZWDs with respect to the GPT models. The ZHDs and ZWDs from the models and those derived from the ERA5 data were

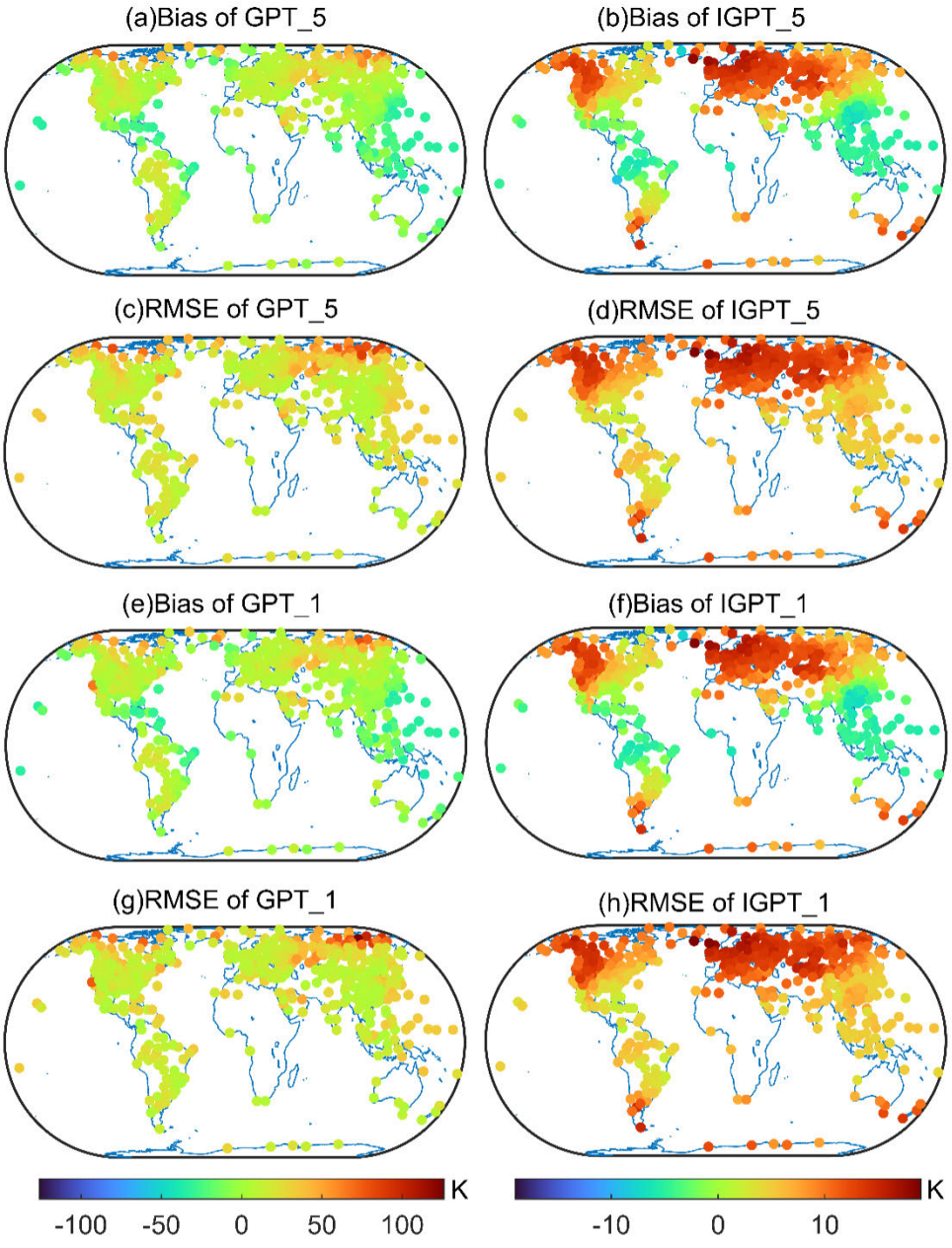

FIGURE 10. Biases and RMSEs of the differences between the RS-derived and model-derived *T* from GPT minus RS and IGPT minus RS calculated for 512 RS stations at the 10 km level in 2019 (unit: K).

compared vertically at different heights. As shown in Fig. 11, for the GPT models, the values of ZHD Biases increased significantly as altitude increased, whereas the values of ZHD Biases of the IGPT models are far smaller than those of the GPT models, particularly at higher altitudes (see Fig. 12(a)). Apparent positive Biases can be observed in the GPT models, but the IGPT models mainly have negative Biases. Fig. 12(b) shows the height distributions of the ZHD RMSE of the different models, from which it can be observed that at the surface level, the uncertainties of all models are very close to each other. However, the ZHD RMSEs of the GPT models increase along the entire height range with increasing altitude, and the mean RMSEs reach up to 80 mm at a height level of 10 km. For the IGPT models, the ZHD RMSEs decrease with increasing height within a height range of 0∼3 km, and are maintained at the same level when the height is up to 3 km (∼17 mm).

In terms of the ZWD, the surface level is characterized by a large underestimation of the ZWD, and the mean Biases of the 5 deg and 1 deg models are −7 mm and −6.7 mm, respectively; see Fig. 12(c). As the altitude increases, the mean Bias values of the GPT models increase, crossing the zero line for

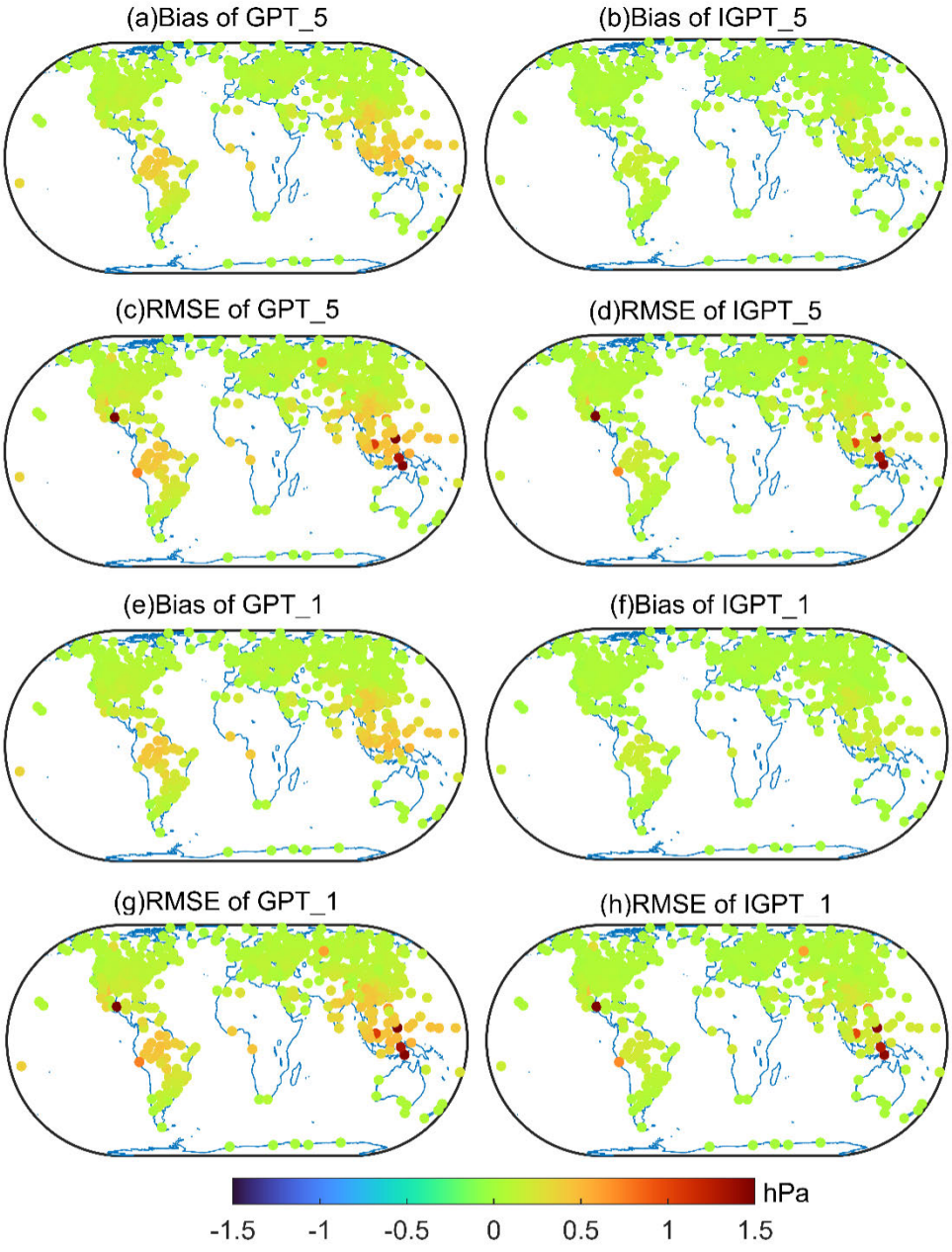

FIGURE 11. Biases and RMSEs of the differences between the RS-derived and model-derived *e* from GPT minus RS and IGPT minus RS calculated for 512 RS stations at the 10 km level in 2019 (unit: hPa).

middle altitudes and presenting a slight overestimation for higher altitudes (maintained at the same level of ∼1.5 mm); however, for the IGPT models, the values of Biases tend to zero when the height is up to 2 km. Interestingly, the absolute values of the GPT models decrease with increasing height more than those of the IGPT models. This is mainly because the overestimation of P with increasing height caused by the isothermal model leads to the overestimation of e (see (8)), and consequently to overestimating the ZWDs of the GPT models (see (7)), which is the reason why the ZWDs of the GPT models are closer to the reference data than those of the IGPT models below a height of 2 km; see Fig. 12(d). Hence to minimize the RMSE it is imperative that the Biases of the ZWD be reduced to as little as possible for the IGPT models.

Figs. 13 and 14 illustrate the global distribution of Biases and RMSEs of the differences between ERA5-derived and model-derived ZHDs. Only the results of height levels 0 (Fig.13) and 10 (Fig. 14) are given since they represent the cases with the minimum and maximum altitude, and the figures of other cases are similar to them. As displayed in Fig. 13, the distributions of both Biases and RMSEs

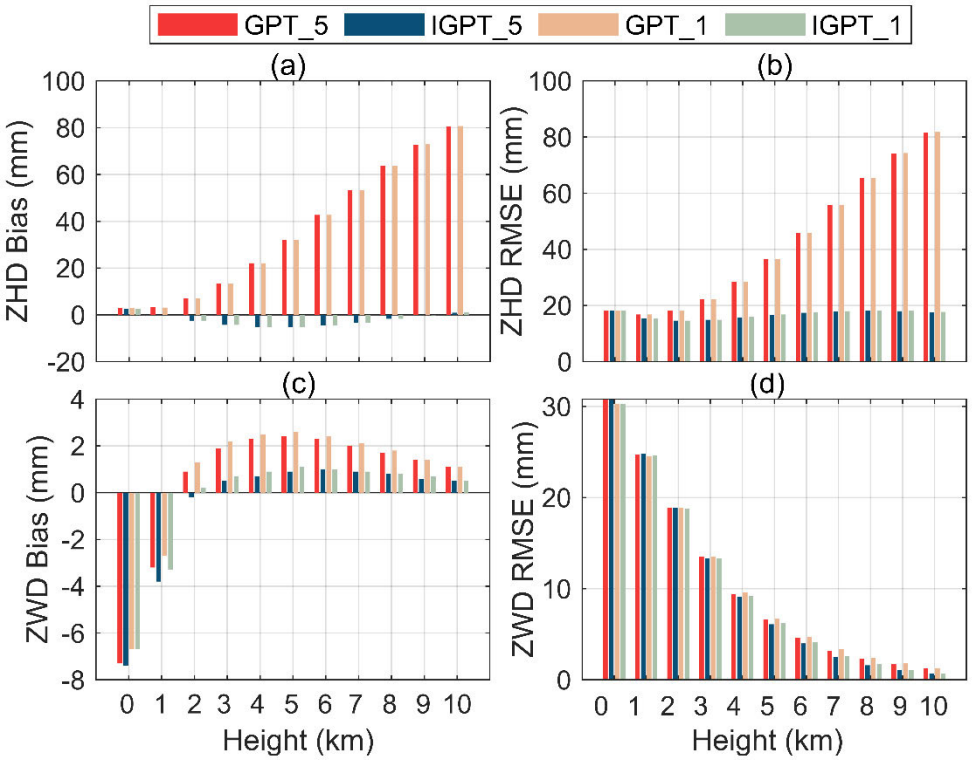

FIGURE 12. Error statistics of the GPT and IGPT models per level. The Bias and RMSE differences between the zenith tropospheric delays are provided by ERA5 data and models in mm for 360 × 181 grid points analyzed at each level. (a): Biases of ZHD at different levels (unit: mm); (b): RMSEs of ZHD at different levels (unit: mm); (c) Biases of ZWD at different levels (unit: mm); and (d): RMSEs of ZWD at different levels (unit: mm).

show typical latitudinal variations for all models; the positive Biases are mainly distributed in low-latitude regions, negative Biases are mainly distributed in high-latitude regions, and values of the RMSEs vary in a wavy manner with respect to latitude (i.e., small values are distributed at horse latitudes and large values are distributed at low and high latitudes). Large RMSE values were observed over the Antarctic Ocean, probably due to the complex atmospheric turbulence caused by the Antarctic circumpolar current (ACC) system [32], and in the northern Atlantic and Pacific Oceans, which is consistent with the results of Mateus *et al.* [33]. However, for the GPT_5 model, the Biases and RMSEs are relatively large in some high-altitude regions (e.g., the Himalayas and Andes). This is mainly caused by the larger altitude differences between the grid point of ERA5 data and the corresponding four grid points of the model, which in combination with using the isothermal model to conduct the vertical correction implicates the larger uncertainties of ∼45 mm. The marked RMSE in the GPT_5 model is reduced to only 15 mm by the IGPT_5 model.

With the overestimation of pressure caused by the isothermal model, particularly at a height level of 10 km, the GPT models show large warm Biases on a global scale (see Fig. 14(a, e)), and the distribution of RMSEs is similar to that of Biases (see Fig. 14(c, g)). For the IGPT models, the negative Biases are mainly distributed in low-latitude regions and the positive Biases are mainly distributed in high-latitude regions (see Fig. 14(b, f)), which is the opposite of the Bias distribution at the surface level. This may be due to the uncertainty of the new dT model, which only takes the latitudinal and annual variations in lapse rates into account. The accuracies of the GPT models become particularly poor at a height level of 10 km, and the ranges of RMSEs are from 28 to 113 mm and from 28 to 108 mm for the GPT_5 and GPT_1 models, respectively, whereas the IGPT models achieve good RMSE results with ranges from 2 to 39 mm and from 2 to 37 mm for the IGPT_5 and IGPT_1 models respectively, at this height level (see Fig. 14(d, h)). Furthermore, 72% of the grid points of the GPT models had RMSEs greater than 80 mm, but for the IGPT models, the percentage < 20 mm was 69%. The mean RMSEs of the GPT and IGPT models are 82 mm and 18 mm, respectively. Thus, the precision improvement of the IGPT models compared with the GPT models is 78%.

In terms of ZWDs, analogous plots of the Biases and RMSEs are depicted in Figs. 15 and 16. As displayed in Fig. 15, all models show a similar distribution to each other for both Biases and RMSEs at the surface level and have negative Biases in many areas (the percentage reaches 96%), showing a systematic underestimation of ZWDs for GPT.

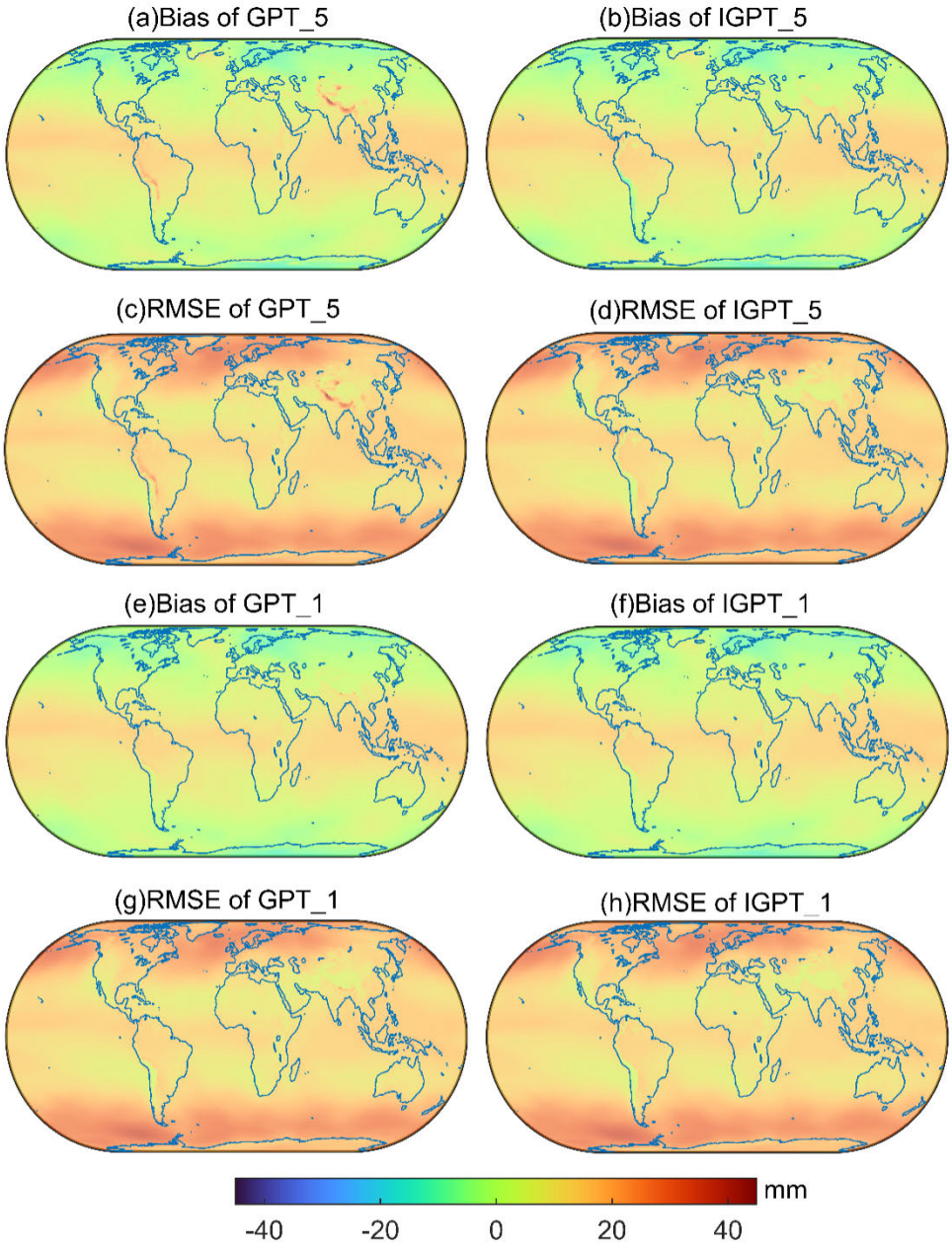

FIGURE 13. Global distribution of the ZHD Biases and RMSEs in the two types of models tested by using the ERA5 data at the surface level (unit: mm).

The distribution of RMSEs is mostly altitude-dependent, with larger values appearing in low-altitude regions (e.g., most sea areas, Australia, eastern China and eastern South America and North America) and small values appearing in high altitude regions (e.g., Antarctica, Greenland, Qinghai-Tibet Plateau, and western America). This difference could be explained by the fact that the water vapor in the atmosphere decreases with increasing altitude. Unexpectedly, some abnormal values of RMSEs appear in high altitude regions, e.g., the values reach up to approximately 232 mm and 90 mm for GPT_5 and GPT_1, respectively, in the Himalayas. This indicates that the horizontal resolution of 1° for the GPT_1 model is apparently not sufficient to capture microclimate, particularly in complex terrain, not to mention the GPT_5 model with a horizontal resolution of 5°. Benefitting from the new dT model and the adiabatic model, the maximum values of IGPT_5 and IGPT_1 are reduced from 232 to 190 mm and from 90 to 76 mm, respectively. This demonstrates the effectiveness of the IGPT models in the vertical correction of ZWDs.

Fig. 16 shows the global Biases and RMSEs of ZWDs for all models at an altitude of 10 km. Due to the overestimation

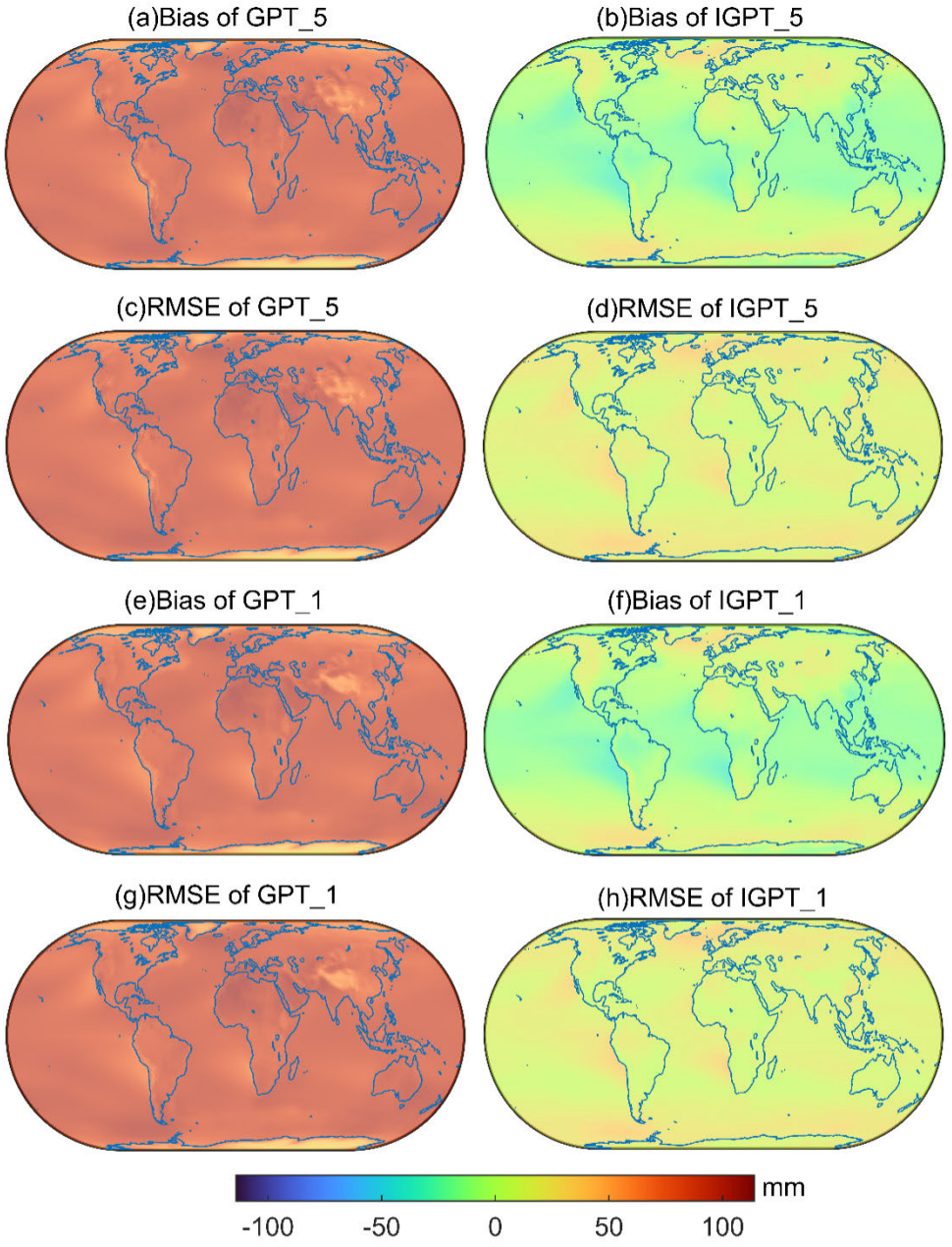

FIGURE 14. Global distribution of the ZHD Biases and RMSEs in the two types of models tested by using the ERA5 data an height level of 10 km (unit: mm).

of e caused by the isothermal model, the GPT models significantly overestimate the ZWD over the tropical region, achieving a maximum RMSE of 9 mm for GPT_5 and a maximum RMSE of 8 mm for GPT_1. This effect is reduced by the IGPT models with maximum RMSEs of 5 mm and 4 mm for the IGPT_5 and IGPT_1 models, respectively. Moreover, the RMSEs of the IGPT models are smaller than those of the GPT models worldwide, especially over tropical regions. These results also indicate the superiority of the IGPT models compared with the GPT models in the vertical correction of ZWDs.

C. PERFORMANCE OF THE IGPT AND GPT MODELS IN GNSS APPLICATIONS

A total of 409 globally distributed IGS stations in 2019 were selected to further substantiate the performances of the GPT and IGPT models in predicting zenith tropospheric delays. To extract ZWDs from the IGS ZTDs, we derived ZHDs from the NCEP data in 2019 by the integration method used in section B for each station. Subsequently, the ZWD can be obtained by ZTD_{IGS} minus ZHD_{NCEP}. Then, the values of the ZWDs and ZHDs for each station were treated as reference values to validate the two types of models.

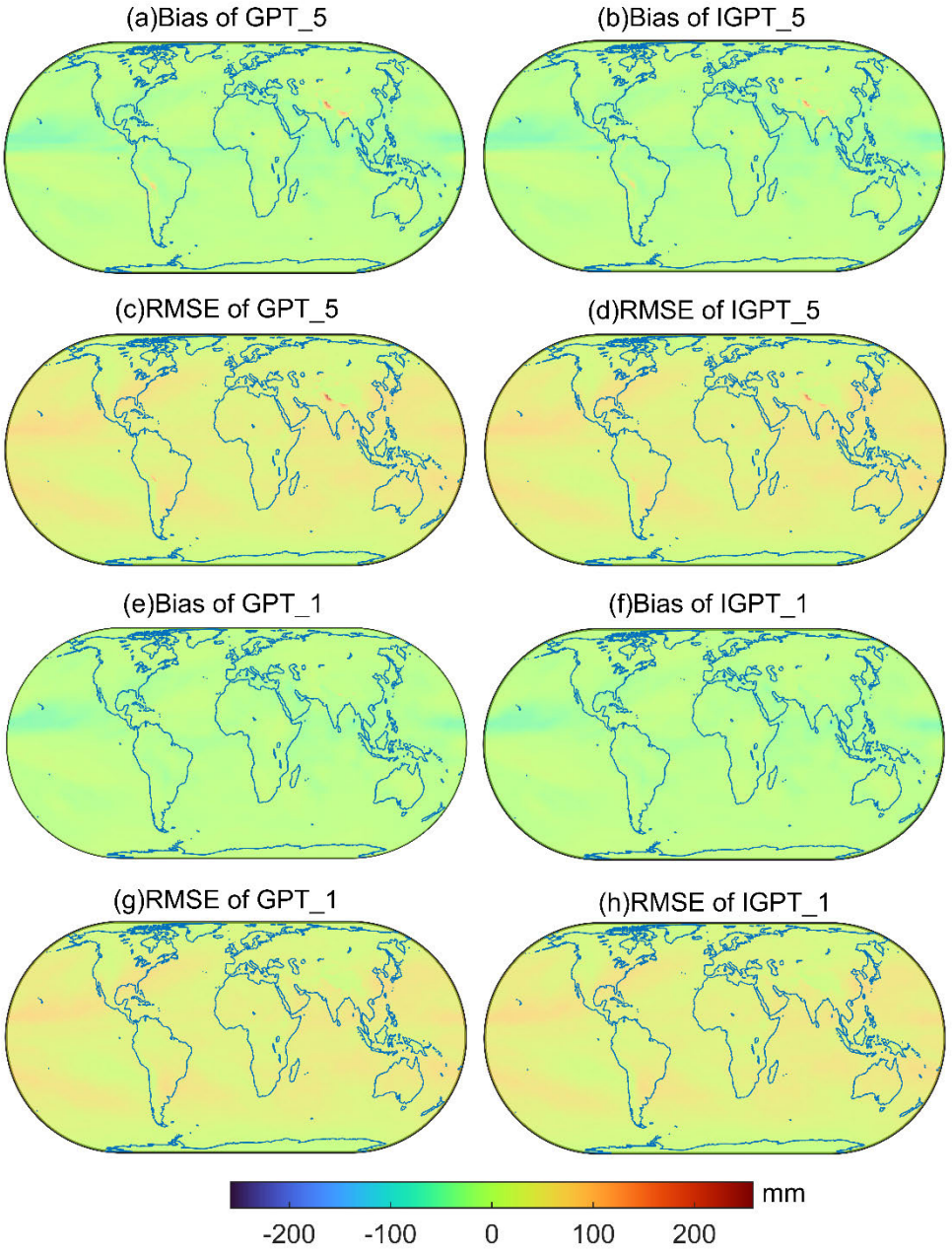

FIGURE 15. Global distribution of the ZWD Biases and RMSEs in the two types of models tested by using the ERA5 data at the surface level (unit: mm).

The values of the Bias and RMSE for the GPT and IGPT models are summarized in **Table 3**. The statistical results of the IGPT models, including RMSE and Biases, are better than those of the GPT models. The mean $Bias_{ZHD}$ and $RMSE_{ZHD}$ of IGPT_1 are reduced from 4.0 to 3.5 mm and from 15.6 to 15.3 mm, respectively, and those of IGPT_5 are reduced from 4.2 to 3.1 mm and from 15.7 to 15.1 mm, respectively. The improvement effects of IGPT_5 are better than those of IGPT_1, which may be caused by the fact that the altitude differences between the IGS stations and the corresponding four grid points of IGPT_5 are greater than those between the IGS stations and IGPT_1. In terms of the ZWD, all models obviously underestimate wet delays, which agrees with the results from the comparison of ZWDs to ERA5 data. The two 1° grid models are equivalent in the mean $RMSE_{ZWD}$ and $Bias_{ZWD}$ as well as their ranges, whereas the absolute value of the mean $Bias_{ZWD}$ of IGPT_5 is slightly larger than that of GPT_5, but the maximum of $Bias_{ZWD}$ and $RMSE_{ZWD}$ are reduced from 112.1 to 92.2 mm and from 120.5 to 100.3 mm, respectively, by the IGPT_5 model. Presumably, this stems from the fact that the adiabatic model reduces the ZWDs derived from the isothermal model, resulting in where the

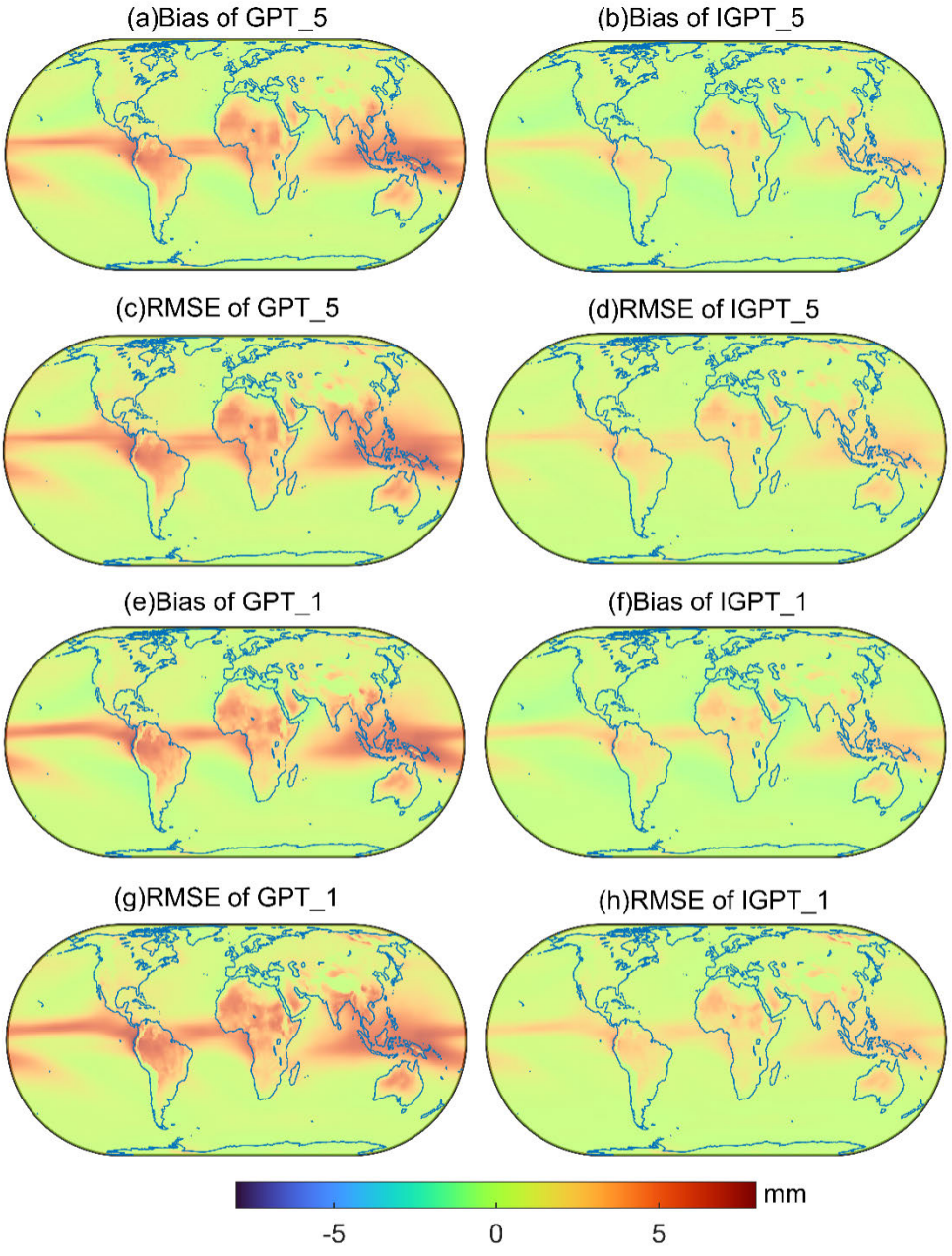

FIGURE 16. Global distribution of the ZWD Biases and RMSEs in the two types of models tested by using the ERA5 data at an height level of 10 km (unit: mm).

ZWD is overestimated, the absolute values of Bias decrease, and where the ZWD is underestimated increase.

The average altitude differences between the IGS stations and the corresponding four grid points of the two types of models are counted, and the changes in the stationwise differences in the RMSE and Bias values with the altitude difference are plotted in Fig. 16. Residuals of Biases reckoned in the sense of ''IGPT minus GPT in ZHD'' and ''IGPT minus GPT in ZWD'' are almost continuously with a negative sign (see Fig. 17(a, c)), confirming that the IGPT models reduce both ZHDs and ZWDs derived from the GPT models and that the greater the altitude difference is, the more obvious the reduction. In terms of RMSEs, residuals reckoned in the sense of ''IGPT minus GPT in ZHD'' are also mostly negative (see Fig. 17(b, d)), suggesting that the IGPT models act to redress specific shortcomings of the GPT models in the regions with large altitude differences. The maximum reduction is 19.0 mm from 23.1 to 4.1 mm at the MKEA station (Mauna Kea, United States).

Interestingly, the uncertainty of the IGPT models in ZWD estimations looks like it depends on whether the height difference is positive or negative (see Fig. 17(b, d)); e.g., as the underestimation of ZWDs of the GPT models appears where the height difference is positive, the corresponding RMSE

TABLE 3. Error statistics of the GPT and IGPT models. The Bias and RMSE differences between the zenith tropospheric delays are provided by the IGS and models in mm for 395 IGS stations analyzed over the 2019 period (unit: mm).

Models	$bias_{ZHD}$	$RMSE_{ZHD}$	$bias_{ZWD}$	$RMSE_{ZWD}$
GPT_5	4.2[-14.1 28.0]	15.7[5.5 29.6]	-5.6[-60.1 112.1]	37.1[7.0 120.5]
IGPT_5	3.1[-14.1 16.9]	15.1[2.0 29.6]	-5.9[-60.1 92.2]	37.1[7.0 100.3]
GPT_1	4.0[-12.1 23.1]	15.6[5.8 29.6]	-4.3[-62.0 24.6]	36.1[7.1 70.5]
IGPT_1	3.5[-12.1 16.8]	15.3[4.8 29.6]	-4.3[-62.0 24.6]	36.1[7.1 70.5]

Values within square brackets are the minimum and maximum

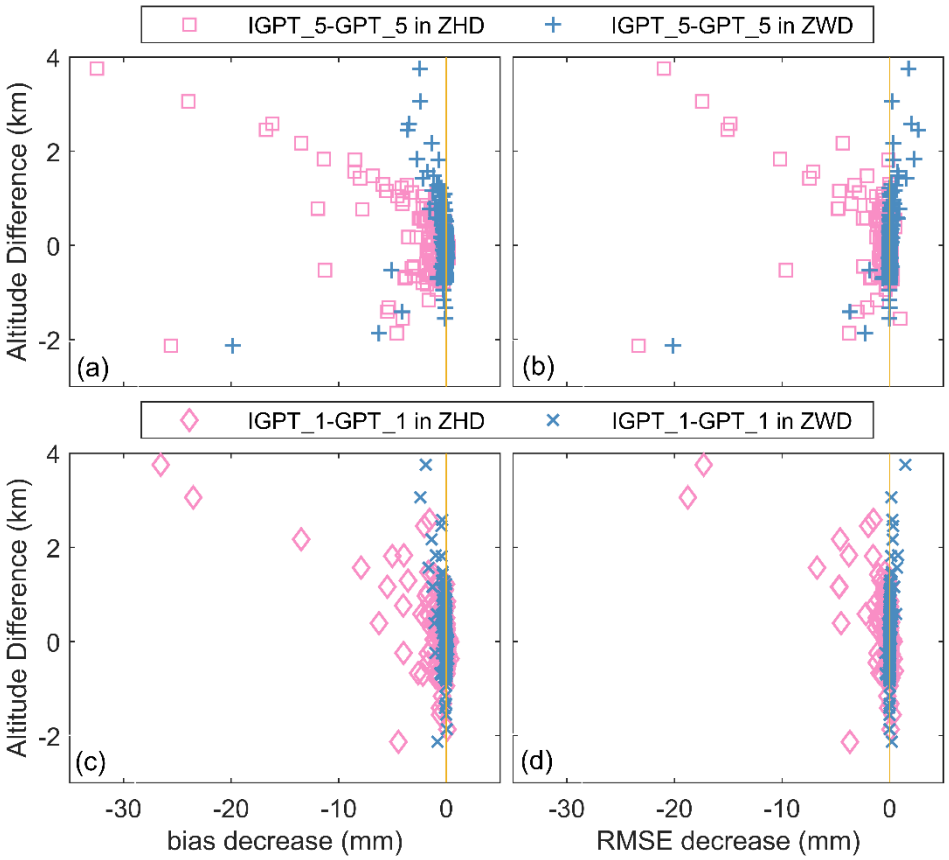

FIGURE 17. Change in the Bias and RMSE with the altitude difference for the GPT and IGPT models (unit: mm). This shows that the performance of the IGPT model in ZHD predictions improves significantly with increasing altitude difference. (a): Bias decrease of the 5° grid model (unit: mm); (b): RMSE decrease of the 5° grid model (unit: mm); (c) Bias decrease of the 1° grid model (unit: mm); and (d): RMSE decrease of the 1° grid model (unit: mm).

values of the IGPT models become slightly larger, and as the overestimation of ZWDs of the GPT models appears where the height difference is negative, the corresponding RMSE values of the IGPT models become smaller. This phenomenon is especially obvious for IGPT_5, with a maximum reduction of 20.0 mm at the IQQE station (Iquique, Chile). The results are consistent with those from the comparison of ZWDs to ERA5 data and prove once again the necessity of correcting the systematic underestimation of the ZWD for the GPT models.

IV. CONCLUSION

As the temperature lapse rates of the GPT models are derived from the lowest two pressure levels of the ECMWF data and the isothermal model is utilized in pressure reductions, the application of the GPT models is limited to the lower atmosphere. Therefore, the development of the GPT models, namely, the IGPT models, was proposed by using 10 years of 6 h pressure-level data from NCEP. The process of modeling the temperature lapse rate was described in detail. The mean values and annual amplitudes for the temperature lapse rate, were determined and analyzed, and stored in a look-up table. Furthermore, we redefined the expression of the pressure reduction used in the GPT models considering adiabatic effects in the real atmosphere.

Comprehensive comparisons between the GPT and IGPT models were conducted by using globally distributed radiosonde data and ERA5 data, as well as GNSS data.

The comparisons with the meteorological parameters (i.e., T, P, and e) derived from the radiosonde data show that altitude seriously affects the accuracy of the GPT models, and the IGPT models can effectively reduce this effect. The statistical results show that the RMSE values of the GPT models for all meteorological parameters were very close to those of the IGPT models at lower altitudes, but with increasing altitude, they increased significantly, whereas those of the IGPT models were relatively stable and small. The IGPT models achieved the precision improvements of approximately 58%, 79%, and 39% for T, P, and e, respectively, compared with the GPT models at the 10 km level. In comparison with the ZTDs derived from the ERA5 data, the IGPT models outperformed the GPT models over the entire height range (0∼10 km) in ZHD corrections, e.g., at a height of 10 km, the IGPT models had a mean $RMSE_{ZHD}$ value of 17 mm, outperforming the GPT models (with a mean RMSE of 80 mm), which was an approximately 79% improvement. In terms of ZWDs, the effectiveness of the IGPT models in vertical correction was also demonstrated. Additionally, the zenith delays were also compared against the IGS delays to further verify whether the estimations from the IGPT models were truly more realistic. The results showed that the IGPT models could improve the $bias_{ZHD}$ and $RMSE_{ZHD}$ at most IGS stations, particularly for the large altitude differences between the IGS stations and the corresponding four grid points of the model. These improved models are highly recommended to obtain high-precision ZHD estimations for high-precision GNSS positioning and GNSS meteorology, where the ZHD is obtained by a priori model but the ZWD is estimated as an extra-tropospheric parameter alongside position coordinates. Due to the systematic underestimation of e at the surface, the IGPT models have little or no improvement in ZWD predictions below a height of 2 km. However, for some ZWD overestimated IGS stations, the improvement of the IGPT models is obvious, particularly for the IGPT_5 model.

In summary, the validation results indicate that the GPT models may have weaknesses when correcting meteorological parameters over a large height difference, whereas the IGPT models still have good performance when the height difference is large; thus, these improved models are very useful for estimating meteorological parameters or tropospheric delays in areas of complex terrain and for certain applications where the correction of a long vertical distance is necessary (e.g., airborne positioning). Further development of these IGPT models is underway, and are aimed at exploring the causes of the systematic underestimation of ZWDs to improve the ZWD model.

ACKNOWLEDGMENT

The authors would like to thank the VMF Data Server for providing the GPT3 Model (access at: https://vmf.geo.tuwien.ac.at/codes/), the National Centre for Environmental Prediction for providing access to the web-based NCEP reanalysis data, the European Centre for Medium-Range Weather Forecasts for providing the ERA5 data, the University of Wyoming for providing the radiosonde data, and the International GNSS Service for providing the final tropospheric zenith delay data.

REFERENCES

[1] J. Böhm, G. Möller, M. Schindelegger, G. Pain, and R. Weber, "Development of an improved empirical model for slant delays in the troposphere (GPT2w)," *GPS Solutions*, vol. 19, no. 3, pp. 433–441, Jul. 2015.
[2] E. Krueger, T. Schuler, and B. Arbesser-Rastburg, "The standard tropospheric correction model for the European satellite navigation system Galileo," in *Proc. Gen. Assem. Int. Union Radio Sci. (URSI)*, New Delhi, India, Oct. 2005, pp. 1–4.
[3] T. Schüler, "The TropGrid2 standard tropospheric correction model," *GPS Solutions*, vol. 18, no. 1, pp. 123–131, Jan. 2014.
[4] J. Böhm, R. Heinkelmann, and H. Schuh, "Short note: A global model of pressure and temperature for geodetic applications," *J. Geodesy*, vol. 81, no. 10, pp. 679–683, 2007.
[5] K. Lagler, M. Schindelegger, J. Böhm, H. Krasna, and T. Nilsson, "GPT2: Empirical slant delay model for radio space geodetic techniques," *Geophys. Res. Lett.*, vol. 40, no. 6, pp. 1069–1073, Mar. 2013.
[6] D. Landskron and J. Böhm, "VMF3/GPT3: Refined discrete and empirical troposphere mapping functions," *J. Geodesy*, vol. 92, no. 4, pp. 349–360, Apr. 2018.
[7] W. Li, Y. Yuan, J. Ou, H. Li, and Z. Li, "A new global zenith tropospheric delay model IGGtrop for GNSS applications," *Chin. Sci. Bull.*, vol. 57, no. 17, pp. 2132–2139, Jun. 2012.
[8] W. Li, Y. Yuan, J. Ou, Y. Chai, Z. Li, Y.-A. Liou, and N. Wang, "New versions of the BDS/GNSS zenith tropospheric delay model IGGtrop," *J. Geodesy*, vol. 89, no. 1, pp. 73–80, Jan. 2015.
[9] J. Saastamoinen, "Atmospheric correction for the troposphere and stratosphere in radio ranging satellites," *Artif. Satell. Geodesy*, vol. 15, pp. 247–251, Jan. 1972.
[10] J. Askne and H. Nordius, "Estimation of tropospheric delay for microwaves from surface weather data," *Radio Sci.*, vol. 22, no. 3, pp. 379–386, May 1987.
[11] G. Möller, R. Weber, and J. Böhm, "Improved troposphere blind models based on numerical weather data," *Navigation*, vol. 61, no. 3, pp. 203–211, Sep. 2014.
[12] X. Wang, K. Zhang, S. Wu, S. Fan, and Y. Cheng, "Water vapor-weighted mean temperature and its impact on the determination of precipitable water vapor and its linear trend," *J. Geophys. Res., Atmos.*, vol. 121, pp. 833–852, Jan. 2016.
[13] J. Z. Kalita and Z. Rzepecka, "Impact of the initial tropospheric zenith path delay on precise point positioning convergence during active conditions," *Meas. Sci. Technol.*, vol. 28, no. 4, Apr. 2017, Art. no. 045102.
[14] H. Zhang, Y. Yuan, W. Li, J. Ou, Y. Li, and B. Zhang, "GPS PPP-derived precipitable water vapor retrieval based on T_m/P_s from multiple sources of meteorological data sets in China," *J. Geophys. Res., Atmos.*, vol. 122, no. 8, pp. 4165–4183, Apr. 2017.
[15] F. Zheng, Y. Lou, S. Gu, X. Gong, and C. Shi, "Modeling tropospheric wet delays with national GNSS reference network in China for BeiDou precise point positioning," *J. Geodesy*, vol. 92, no. 5, pp. 545–560, May 2018.
[16] Y. Yao, Z. Sun, and C. Xu, "Establishment and evaluation of a new meteorological observation-based grid model for estimating zenith wet delay in ground-based global navigation satellite system (GNSS)," *Remote Sens.*, vol. 10, no. 11, p. 1718, Oct. 2018.
[17] Z. Liu, X. Chen, and Q. Liu, "Estimating zenith tropospheric delay based on GPT2w model," *IEEE Access*, vol. 7, pp. 139258–139263, 2019.
[18] F. Yang, J. Guo, X. Meng, J. Shi, D. Zhang, and Y. Zhao, "An improved weighted mean temperature (T_m) model based on GPT2w with T_m lapse rate," *GPS Solutions*, vol. 24, no. 2, Apr. 2020, Art. no. 46.
[19] Q. Zhao, W. Yao, Y. Yao, and X. Li, "An improved GNSS tropospheric tomography method with the GPT2w model," *GPS Solutions*, vol. 24, no. 2, pp. 3764–3771, Apr. 2020.
[20] J. Chen, J. Wang, A. Wang, J. Ding, and Y. Zhang, "SHAtropE—A regional gridded ZTD model for China and the surrounding areas," *Remote Sens.*, vol. 12, no. 1, p. 165, Jan. 2020.
[21] F. Yang, J. Guo, X. Meng, J. Shi, and L. Zhou, "Establishment and assessment of a new GNSS precipitable water vapor interpolation scheme based on the GPT2w model," *Remote Sens.*, vol. 11, no. 9, p. 1127, May 2019.
[22] C. Jiang, T. Xu, S. Wang, W. Nie, and Z. Sun, "Evaluation of zenith tropospheric delay derived from ERA5 data over China using GNSS observations," *Remote Sens.*, vol. 12, no. 4, p. 663, Feb. 2020.

[23] J. Mao, Q. Wang, Y. Liang, and T. Cui, "A new simplified zenith tropospheric delay model for real-time GNSS applications," *GPS Solutions*, vol. 25, no. 2, p. 43, Apr. 2021.
[24] Y. Yao, Z. Sun, C. Xu, L. Zhang, and Y. Wan, "Development and assessment of the atmospheric pressure vertical correction model with ERA-interim and radiosonde data," *Earth Space Sci.*, vol. 5, no. 11, pp. 777–789, Nov. 2018.
[25] T. Li, L. Wang, R. Chen, W. Fu, B. Xu, P. Jiang, J. Liu, H. Zhou, and Y. Han, "Refining the empirical global pressure and temperature model with the ERA5 reanalysis and radiosonde data," *J. Geodesy*, vol. 95, no. 3, pp. 1–7, Mar. 2021.
[26] A. E. Niell, "Global mapping functions for the atmosphere delay at radio wavelengths," *J. Geophys. Res., Solid Earth*, vol. 101, no. B2, pp. 3227–3246, 1996.
[27] S. J. Marshall, M. J. Sharp, D. O. Burgess, and F. S. Anslow, "Near-surface-temperature lapse rates on the Prince of Wales Icefield, Ellesmere Island, Canada: Implications for regional downscaling of temperature," *Int. J. Climatol.*, vol. 27, no. 3, pp. 385–398, 2007.
[28] L. Gao, M. Bernhardt, K. Schulz, and X. Chen, "Elevation correction of ERA-Interim temperature data in the Tibetan Plateau," *Int. J. Climatol.*, vol. 37, no. 9, pp. 3540–3552, 2016.
[29] A. S. Gardner, M. J. Sharp, R. M. Koerner, C. Labine, S. Boon, S. J. Marshall, D. O. Burgess, and D. Lewis, "Near-surface temperature lapse rates over Arctic glaciers and their implications for temperature downscaling," *J. Climate*, vol. 22, no. 16, pp. 4281–4298, Aug. 2009.
[30] F. Kleijer, "Troposphere modeling and filtering for precise GPS leveling," Netherlands Geodetic Commission, Delft, The Netherlands, Tech. Rep., 2004, vol. 56.
[31] K. Wilgan, W. Rohm, and J. Bosy, "Multi-observation meteorological and GNSS data comparison with numerical weather prediction model," *Atmos. Res.*, vol. 156, pp. 29–42, Apr. 2015.
[32] S. R. Rintoul, C. W. Hughes, and D. Olbers, "The Antarctic circumpolar current system," *Int. Geophys.*, vol. 77, p. 271, Jan. 2001.
[33] P. Mateus, J. Catalão, V. B. Mendes, and G. Nico, "An ERA5-based hourly global pressure and temperature (HGPT) model," *Remote Sens.*, vol. 12, no. 7, p. 1098, Mar. 2020.

JIAN MAO received the B.S. degree in surveying engineering from Henan Polytechnic University, Henan, China, in 2008, and the Ph.D. degree in cartography and geography information system from Nanjing Normal University, Nanjing, China, in 2015. He is currently a Lecturer with Tianjin Normal University. His main research interests include global navigation satellite system atmospheric meteorological studies, and GNSS/MET and high precision GNSS data processing.

JUNYANG HAN received the bachelor's degree in geographic information system from Tianjin Normal University, in 2019, where she is currently pursuing the master's degree in physical geography. Her main research interest includes atmospheric meteorology research.

TIEJUN CUI received the Ph.D. degree in geodesy from the Universität der Bundeswehr München, Germany, in 1998. He is currently a Professor with the School of Geographic and Environmental Sciences, Tianjin Normal University, Tianjin, China. His research interests include multi-source spatial data fusion, location-based information service, and smart city.